

Chaperonin Containing TCP-1 Protein Level in Breast Cancer Cells Predicts Therapeutic Application of a Cytotoxic Peptide

Rania Bassiouni¹, Kathleen N. Nemeč¹, Ashley Iketani¹, Orielyz Flores², Anne Showalter¹, Amr S. Khaled³, Priya Vishnubhotla³, Robert W. Sprung Jr⁴, Charalambos Kaittanis⁵, Jesus M. Perez⁶, and Annette R. Khaled¹

Abstract

Purpose: Metastatic disease is a leading cause of death for patients with breast cancer, driving the need for new therapies. CT20p is a peptide previously discovered by our group that displays cancer-specific cytotoxicity. To design the optimal therapeutic use of the peptide, we identified the intracellular target of CT20p in breast cancer cells, correlating expression patterns of the target with susceptibility to CT20p.

Experimental Design: Using polymeric nanoparticles to deliver CT20p, we assessed cytoskeletal changes, cell migration, adhesion, and viability in cells treated with the peptide. Protein pull-down experiments, coupled to mass spectrometry, enabled identification of the peptide's intracellular target. Biochemical and histologic techniques validated target identity in human cell lines and breast cancer tissue microarrays and revealed susceptibility patterns to CT20p.

Results: Chaperonin containing TCP-1 (CCT) was identified as the intracellular target of CT20p. Cancer cells susceptible to CT20p had increased CCT, and overexpression of CCT β , a subunit of the CCT complex, enhanced susceptibility to CT20p. Susceptible cells displayed reduced tubulin, a substrate of CCT, and inhibition of migration upon CT20p treatment. CCT β levels were higher in invasive ductal carcinomas than in cancer adjacent tissues and increased with breast cancer stage. Decreased breast cancer patient survival correlated with genomic alternations in CCT β and higher levels of the chaperone.

Conclusions: Increased CCT protein in breast cancer cells underlies the cytotoxicity of CT20p. CCT is thus a potential target for therapeutic intervention and serves as a companion diagnostic to personalize the therapeutic use of CT20p for breast cancer treatment. *Clin Cancer Res*; 22(17); 4366–79. ©2016 AACR.

Introduction

Breast cancer is the second leading cause of death in women (1); a trend that is mirrored worldwide (2, 3). Although early diagnosis followed by treatment reduces the mortality associated with breast cancer, patient survival and therapeutic options significantly decrease once the cancer disseminates beyond the breast. Triple-negative breast cancer (TNBC) is an especially aggressive disease, with fewer treatment choices due to the absence of estrogen (ER), progesterone (PR), and Her2 receptors. By addressing gaps in the treatment repertoire, new therapies that can be partnered with a

companion diagnostic would have the most impact on patient survival.

To develop a novel cancer therapeutic, we studied the membrane-binding activities of Bax, an apoptotic member of the Bcl-2 family (4), and discovered that a peptide derived from the C-terminus of Bax, CT20p, had inherent cytotoxic activity (5). Death induced by CT20p was independent of caspase inhibition, Bax deficiency, and Bcl-2 overexpression (5), suggesting that the unique amphipathic nature of CT20p could be responsible for its cytotoxicity. In the presence of artificial large unilamellar vesicles (LUV) composed of mitochondrial-like lipids, CT20p adopted an $\alpha\beta$ secondary structure and formed pores that released small molecules from the LUVs (5–7). However, we found CT20p to be impermeable to the plasma membrane of mammalian cells (5). Intracellular delivery of the peptide was achieved with nanoparticles (5). The hydrophobic nature of CT20p enabled efficient encapsulation within nanoparticles formed by a novel hyperbranched polyester polymer (HBPE-NPs; refs. 5, 8, 9). Nanoparticle encapsulation protected the peptide from degradation in serum and increased its stability during circulation in host animals, allowing the peptide to be released within cells in a pH- and esterase-dependent manner (8). CT20p-HBPE-NPs caused cancer cell death *in vitro* and *in vivo*, inhibiting and regressing tumors derived from human breast cancer cells implanted in mice (5, 9). Importantly, cancer cells tested were susceptible to the cytotoxic effects of CT20p-HBPE-NPs, whereas normal epithelial cells were resistant (9).

¹Burnett School of Biomedical Science, College of Medicine, University of Central Florida, Orlando, Florida. ²Nanoscience Technology Center, University of Central Florida, Orlando, Florida. ³Orlando VA Medical Center, Orlando, Florida. ⁴Proteomics, Moffitt Cancer Center, Tampa, Florida. ⁵Gordon Center for Medical Imaging, Department of Radiology, Massachusetts General Hospital, Boston, Massachusetts. ⁶Cedars-Sinai Medical Center, Los Angeles, California.

Note: Supplementary data for this article are available at Clinical Cancer Research Online (<http://clincancerres.aacrjournals.org/>).

Corresponding Author: Annette R. Khaled, Burnett School of Biomedical Sciences, College of Medicine, University of Central Florida, 6900 Lake Nona Blvd, Orlando, FL 32827. Phone: 407-266-7035; Fax: 407-266-7003; E-mail: annette.khaled@ucf.edu

doi: 10.1158/1078-0432.CCR-15-2502

©2016 American Association for Cancer Research.

Translational Relevance

Triple-negative breast cancer (TNBC) and other aggressive forms of breast cancer have an increased tendency to metastasize and become refractory to treatments. CT20p is a novel therapeutic agent for cancer through its unique mode of action that targets the molecular chaperone, CCT. The amount of CCT in a cell predicts its susceptibility to CT20p. This, coupled with the finding that CCT levels are elevated in human breast cancer and correlate with disease progression, suggests that CCT could be a companion diagnostic that predicts beneficial outcomes of CT20p treatment. Furthermore, as a neoadjuvant treatment, CT20p could reduce tumor size prior to surgery or radiotherapy and may sensitize cancer cells, reducing the need for aggressive chemotherapy. As a result, debilitating side effects associated with current treatments could be reduced. The coupling of CCT as a diagnostic with CT20p as a treatment provides a personalized treatment approach that, to date, is lacking for recurrent cancers like TNBC.

Many anticancer therapeutic peptides are naturally occurring antimicrobial agents (10). Like CT20p, these peptides associate with the mammalian mitochondrial membrane, but not the plasma membrane, and cause apoptotic or necrotic cell death (11, 12). Because of the similarity of CT20p to antimicrobial peptides and its ability to permeabilize lipid vesicles (6, 7), we previously examined whether the cancer-specific cytotoxicity of CT20p was mediated through its actions upon mitochondria. We found that CT20p altered mitochondrial dynamics and trafficking in breast cancer cells, but not in normal breast epithelial cells, causing mitochondrial clustering (9). However, continued study revealed that the biologic effects of CT20p also included loss of cell adhesion that preceded cell death, decreased integrin levels, reduced F-actin, and cytoskeletal disruption (9). These observations indicated that the action of CT20p on mitochondria could be a secondary effect, and its true primary intracellular target and reason for its cancer-specific cytotoxicity remained to be determined.

In this report, we identified the intracellular target of CT20p to be the molecular chaperone called chaperonin containing T-complex polypeptide 1 (CCT), also known as the TCP1 ring complex (TRiC). CCT is a complex composed of two stacked rings, each with eight distinct subunits in fixed positions (13). The cavity formed by the two rings is the site of substrate binding and folding, which occurs in an ATP-dependent manner (14). Early experiments determined that complete deletion of CCT in yeast is lethal (15, 16), and CCT is known to be an essential protein in eukaryotes and may be overexpressed in cancer cells (17). CCT is responsible for folding approximately 15% of cellular proteins (18, 19) and is the obligate chaperone for both actin and tubulin (20–22). Evidence supporting CCT as the target of CT20p include the biologic effects of the peptide upon cytoskeletal elements requiring actin and tubulin and correlation of CCT protein levels in cells with CT20p cytotoxicity. Herein, we show the functional consequences of CT20p binding to CCT that leads to the death of breast cancer cells and suggest that CT20p may be a cancer-selective cytotoxic agent and CCT a viable target for therapeutic intervention.

Materials and Methods

Cell culture and reagents

MDA-MB-231, MDA-MB-231/Luc, and MDA-MB-468 cells were cultured in DMEM (Cellgro) with 10% FBS (Biowest). MDA-MB-436 cells were cultured in Leibovitz L-15 medium (Cellgro) with 20% FBS. BT-549 cells were cultured in RPMI (Cellgro) with 8 μ g/mL insulin (Santa Cruz Biotechnology) and 10% FBS. MCF-10A cells were cultured in mammary epithelial cell growth media (Lonza). MDA-MB-231/Luc cells were obtained from Cell Biolabs, Inc. All other cell lines were obtained from ATCC, and low-passage cells were used for experiments. CT20p (VTIFVAGVLTASLTIWKKMG) and biotin-tagged CT20p were commercially synthesized (Biopeptide Co., Inc) at >98% purity, with the N- and C- terminals capped with acetyl and amine groups, respectively. For delivery to cells, CT20p was encapsulated in hyperbranched polyester nanoparticles (HBPE-NPs) as previously described (5, 8, 9). Typically, a peptide loading of 0.15 μ g CT20p to 1 mg nanoparticle is achieved. Purified recombinant His-tagged CCT β derived from *E. coli* was obtained commercially (MyBioSource) at >90% purity.

Measurement of cell viability

To determine IC₅₀ concentrations of CT20p, cells at 60% confluency were treated with a dose range of CT20p-HBPE-NPs for 48 hours. Cell viability was determined using CellTiter-Glo Luminescent Cell Viability Assay (Promega). IC₅₀ determination was performed with GraphPad Prism software. To determine populations of live, apoptotic, and necrotic cells, cells were treated with CT20p-HBPE-NPs (75- μ g nanoparticles/mL). After defined time points, cell death discrimination was performed with the Sytox AADvanced and F2N12S Violet Ratiometric Apoptosis Kit (Invitrogen). Data were acquired by flow cytometry on a FACS-Canto (BD Biosciences) and analyzed with FCSEXPRESS software (DeNovo).

Calculation of metabolic capacity

Metabolic profiles for each cell line were obtained using a Seahorse XFe24 analyzer, as detailed in Supplementary Materials. Cells were treated with CT20p-HBPE-NPs (75- μ g nanoparticles/mL) for 3 hours before running the assay. Metabolic capacity was defined as the maximum response in both mitochondrial and glycolytic contexts. CT20p-treated results were calculated as a percentage of untreated results.

Immunoblotting

Cell lysates were obtained by mechanical douncing, analyzed by SDS-PAGE, and then transferred to Immobilon-FL membranes (Millipore). Blots were probed with primary antibodies against CCT β (Millipore), CCT δ (Abcam), CCT ϵ (Abcam), or p38 MAPK (Santa Cruz Biotechnology). Detection was performed by incubation with IRDye secondary antibodies (LI-COR), followed by imaging on the Odyssey detection system (LI-COR). Immunoblots were quantified with Image Studio software (LI-COR). Proteins of interest were assessed relative to p38 MAPK loading controls and then normalized to the MCF-10A control cells.

Quantitation of gene expression

RNA was isolated from cells using TRIzol (Invitrogen). cDNA was synthesized using the iScript Advanced cDNA Synthesis Kit (Bio-Rad). Quantitative real-time PCR was performed on a

7900HT Fast Real-Time PCR system (Applied Biosystems). Reactions were prepared in triplicate using SSoAdvanced Universal SYBR Green Supermix (Bio-Rad) and PrimePCR Assays for the following: CCT2, CCT4, CCT5, and GAPDH (Bio-Rad). Levels of CCT subunits were compared with the endogenous control GAPDH. Expression levels were calculated relative to the lowest expressed subunit: CCT4 in MCF-10A cells. Relative expression (RQ) values were calculated using the formulas:

$$\begin{aligned}\Delta CT &= CT \text{ of target gene (CCT)} \\ &\quad - CT \text{ of endogenous gene (GAPDH)} \\ \Delta\Delta CT &= \Delta CT - \Delta CT \text{ of reference gene} \\ &\quad (\text{CCT4 from MCF10A cells}) \\ RQ &= 2^{-\Delta\Delta CT}\end{aligned}$$

Cellular adhesion assay

A standard crystal violet assay was performed (9). Briefly, 96-well tissue culture plates were coated with 20 $\mu\text{g}/\text{mL}$ fibronectin (Sigma). Cells were seeded at a density of 10,000 cells/well and incubated overnight. Cells were treated CT20p-HBPE-NPs at various doses for 48 hours. Plates were washed, fixed, and adhered cells stained with 5 mg/mL crystal violet (Sigma). Absorbance was measured at 595 nm using an EnVision plate reader (Perkin Elmer).

Pull-down experiments

Protein pull-downs were performed with 200- μg protein lysates from MDA-MB-231 and MCF-10A cells by mechanical douncing. Lysates were precleared with streptavidin-agarose beads (Pierce), then incubated with 10 μg of biotin-CT20p or biotin alone for 3 hours at room temperature, followed by overnight incubation at 4°C with streptavidin-agarose beads. Beads were washed with buffer (25 mmol/L Tris, 150 mmol/L NaCl, 0.1% NP40, pH 7.4) and then heated in 4 \times loading buffer (Invitrogen) for analysis by SDS-PAGE and immunoblot for CCT. "In-cell" pull downs were performed by delivering biotin-CT20p encapsulated in HBPE-NPs to cells at a dose of 75- μg nanoparticles/mL. Cells were lysed by douncing, and 200 μg of cell lysate was incubated with streptavidin-agarose beads overnight at 4°C and then analyzed as above. Biotin-CT20p pull-downs (0.1–4 nmol) with recombinant His-tagged CCT β protein (0.1 nmol) were performed in 20 mmol/L Tris-HCl buffer.

Migration assay

Cell migration was assessed with the Oris Cell Migration Assembly Kit (Platypus Technologies). Cells were stained with CellTrace Violet (Life Technologies) before seeding at a density of 30,000 cells per well. Treatments with CT20p-HBPE-NPs (75- μg nanoparticles/mL) began the day following seeding. After 24 hours of treatment, stoppers were removed and cells allowed to migrate for additional time (10 hours for MDA-MB-231 and 20 hours for MCF-10A). After migration, fluorescent images were obtained using a Plate Runner HD (Trophos). Control wells had stoppers removed immediately before imaging to provide the premigration area. Images were analyzed by ImageJ software (NIH). Percentage closure was calculated as [(premigration area – migration area)/premigration area] \times 100.

Fixed-cell immunofluorescence

Cells were seeded on glass coverslips and then treated with CT20p-HBPE-NPs (75- μg nanoparticles/mL) or left untreated for 24 hours. Cells were then stained with Mitotracker Red CMXRos

(Life Technologies) before being fixed and permeabilized. Samples were blocked in normal goat serum (Santa Cruz Biotechnology) before incubation with α -tubulin (DM1A) primary antibody and goat α -mouse IgG-FITC secondary antibody (Santa Cruz Biotechnology). Coverslip mounting media contained DAPI for nuclear staining. Images were obtained with a Zeiss LSM 710 microscope, using a Zeiss 63x Pan-Apocromat oil immersion lens and Zeiss Zen software. To determine average tubulin levels per cell, the amount of FITC fluorescence per region of interest was divided by the number of cells in the field. At least four images containing between five and 12 cells were quantified for each condition. Images were analyzed with Volocity software (Perkin Elmer).

IHC

Lung and liver metastases were induced as described in Supplementary Methods. Mouse organs were harvested and fixed as described previously (23). Tissues were analyzed using anti-CCT β primary antibody (LifeSpan Biosciences). Staining of tissue arrays was performed by a Bond-Max Immunostainer (Leica), with an epitope retrieval buffer of EDTA pH 9.0 and Polymer Refine Detection reagents (Leica). Sequential tissue sections were stained with hematoxylin and eosin reagents (Leica). Human breast cancer tissue arrays were purchased from US Biomax (BR1002a, BR10010b, BR963a, and HBre-Duc150-Sur01). Information about tissue type, tumor grade, and receptor status was provided. Array HBre-Duc150-Sur01 also provided information on survival/deceased status of the patient, as well as duration of monitoring in months. Tissues were stained for CCT β as described above. Scoring of CCT β staining was done by a pathologist (A.S. Khaled) following the guidelines in Supplementary Fig. S1.

Overexpression of CCT β

MCF-10A cells were transiently transfected, using TransIT LT1 reagent (Mirus), with pcDNA-CCT2 (GenScript). To assess protein expression, cells were harvested 24 hours following transfection and subjected to immunoblotting for CCT β . Mock transfection controls were treated with TransIT LT1 reagent. For viability assessment, cells were treated with CT20p-HBPE-NPs (75- μg nanoparticles/mL) for 24 hours. Treatments started 24 hours after transfection.

Statistical analysis and data mining

All experiments were performed at minimum three times, and with at least three technical replicates where appropriate. Representative data are presented in this report. For migration and microscopy experiments, data were analyzed using a Student *t* test to compare treated and untreated results. For scoring of CCT β staining in tissue samples, one-way ANOVA was used to compare staining between the various groups. Survival data were analyzed by log-rank (Mantel–Cox) test. Calculations were performed using GraphPad Prism software (GraphPad). Statistical significance was defined as $P < 0.05$. Interrogation of The Cancer Genome Atlas (TCGA) database was accomplished using the websource cBioPortal for Cancer Genomics (<http://cbioportal.org/>; refs. 24, 25).

Results

CT20p is cytotoxic to TNBC cells

TNBC can be characterized into molecular subtypes, such as basal-like 1 and 2 (BL1, BL2), mesenchymal (M), and

mesenchymal stem-like (MSL), by gene expression profiling (26). On the basis of this information, we assessed the cytotoxicity of CT20p in different TNBC subtypes: MDA-MB-468 (BL1), BT-549 (M), MDA-MB-231 (MSL), and MDA-MB-436 (MSL) cells. As a control, we used the breast epithelial line MCF-10A. For delivery of CT20p to cells, the peptide was encapsulated in HBPE-NPs as described previously (5, 8). Our earlier work showed that dye-loaded HBPE-NPs were not toxic (5, 8, 9) and that nanoparticle uptake was comparable across cell lines (representative data for MDA-MB-231 and MCF-10A cells is shown in Supplementary Fig. S2A and S2B). Hence, all experiments involving CT20p were performed with peptide-loaded HBPE-NPs.

Using the various TNBC cell lines, we determined the IC_{50} concentrations of CT20p-HBPE-NPs (Fig. 1A). MDA-MB-231 cells were killed at the lowest dose of CT20p-HBPE-NPs ($IC_{50} = 57 \mu\text{g/mL}$), followed by MDA-MB-436, with BT-549 cells displaying susceptibility at the highest dose ($IC_{50} = 962 \mu\text{g/mL}$). Supporting information concerning IC_{50} determination is provided in Supplementary Fig. S2C and S2D. We previously showed that MDA-MB-231 cells, but not MCF-10A, were susceptible to killing by CT20p-HBPE-NPs (9). These data are recapitulated in Fig. 1B, using a standard cell death discrimination assay that detects changes in membrane asymmetry and permeability. At the 48-hour time point, about 29% of MDA-MB-231 cells were viable after treatment with CT20p-HBPE-NPs (75 $\mu\text{g/mL}$), compared with 84% of MCF-10A cells. Next, we examined the response of the other TNBC cell lines when similarly treated with CT20p-HBPE-NPs (75 $\mu\text{g/mL}$; Fig. 1C). MDA-MB-436 cells were most susceptible to CT20p, displaying characteristics of cell death as early as 6 hours after treatment. This supported the IC_{50} data (Fig. 1A), indicating that MDA-MB-231 and MDA-MB-436 cells (MSL subtype) were the most susceptible to CT20p. The range of responses to CT20p also suggested that the target of the action of peptide could be a variable factor in cancer cells.

Because we previously observed that CT20p associated with mitochondria (9), we examined whether differences in cellular bioenergetics could account for the effects of CT20p. While we did determine that the TNBC cell lines had different metabolic profiles (Supplementary Fig. S3A–S3D), treatment with the peptide did not appreciably change glycolytic or respiratory capacities in manner that correlated with CT20p-mediated decreases in viability (Fig. 1D and E). For example, CT20p did slightly reduce the glycolytic capacity of BT-549 cells, but these cells were the most resistant to the cytotoxic effects of the peptide. Hence, we concluded that CT20p was unlikely to cause cell death by metabolic disruption.

CT20p associates with the chaperonin CCT

To discover intracellular proteins that interact with CT20p and account for its biologic effects (9), we performed a pull-down experiment using biotin-tagged CT20p (biotin-CT20p). Protein lysates were derived from MDA-MB-231 and MCF-10A cells, and interacting proteins were "pulled-down" for analysis by gel electrophoresis and identification by mass spectrometry. Biotin-CT20p associated with a number of proteins unique to MDA-MB-231 cells not found in MCF-10A (Supplementary Fig. S4A–S4C; Supplementary File). We identified CCT as a protein whose inhibition could result in the cytotoxic effects observed for CT20p, such as cytoskeletal disruption (9). Biotin-CT20p pulled down 7

of the 8 subunits of the CCT complex and numerous CCT client proteins (27–29). CCT is a type II chaperonin, composed of eight individual subunits denoted as alpha, beta, gamma, delta, epsilon, eta, theta, and zeta (CCT1–8 in yeast), and is principally responsible for the folding of actin and tubulin into their native forms (19, 21, 22). To confirm that CT20p associated with CCT, we directly probed cytosolic lysates from the TNBC and MCF-10A cells with biotin-CT20p and confirmed the CT20p–CCT interaction by detecting the beta subunit of CCT (CCT β ; Fig. 2A).

We designed an "in-cell" pull-down assay to determine whether CT20p interacted with CCT within cells. Biotin-CT20p was encapsulated in HBPE-NPs and delivered to MDA-MB-231 and MCF-10A cells. After 3 hours, cells were lysed and biotin-CT20p was recovered with streptavidin beads and the pull-down analyzed for CCT β (Fig. 2B). This experiment revealed two important findings: (i) that the CT20p–CCT interaction occurs intracellularly in MDA-MB-231 cells and is detectable by 3 hours and (ii) that biotin-CT20p could escape from the nanoparticles and enter the cytosolic compartment in a biologically active form. Furthermore, CT20p treatment did not decrease total CCT β protein levels, as shown by examining whole-cell lysates (Fig. 2B). Control HBPE-NPs containing DiI dye did not pull-down CCT β , excluding the possibility that the nanoparticles themselves contributed to the interaction with CCT (Supplementary Fig. S4D and S4E).

Next, we examined whether biotin-CT20p bound directly to the CCT subunits or whether the recovery of CCT in the pull downs was due to an indirect interaction (e.g., through a client protein of CCT). Biotin-CT20p and recombinant His-tagged CCT β protein were mixed in a pull-down experiment in which these were the only components (Fig. 2C). By varying the molar ratio of biotin-CT20p to CCT β , we determined that CT20p does interact directly with CCT β at ratios of 1:1 (faint band at the limit of detection) and higher (Fig. 2C). This does not exclude the possibility of CT20p binding to multiple subunits of the CCT complex (e.g. CCT ϵ), thereby increasing the efficiency of the pull-down when the entire complex is present. The results of the in-cell pull down (Fig. 2B) indicate that the reverse is not true—the quaternary structure of the assembled CCT complex does not mask CT20p binding sites.

CCT levels vary across TNBC cell lines

To assess CCT expression in cells that were susceptible or resistant to CT20p, we assayed the basal protein levels of three CCT subunits: beta (β), delta (δ), and epsilon (ϵ ; ref. 30). MDA-MB-231 and MDA-MB-436 cells had the highest levels of the CCT subunits (Fig. 3A), which was confirmed by replicates and quantified (Fig. 3B). These two cell lines were also the most sensitive to CT20p (Fig. 1), suggestive of a correlation between CCT protein levels and the cytotoxic effect of CT20p. Note, while MDA-MB-231 and MDA-MB-436 had similar amounts of CCT, MDA-MB-231 cells were more sensitive to the cytotoxicity of CT20p. This could result from increased chaperone activity or client proteins like actin or STAT3 that enhance the sensitivity of MDA-MB-231 cells to CCT inhibition. We next tested an *in vivo* metastasis model to evaluate CCT levels in the disease state. Intravenous administration of MDA-MB-231/Luc cells via tail vein injection in NOD-SCID-gamma (NSG) mice resulted in lung and liver metastases (ref. 31; Supplementary Fig. S5). Using this model, we examined the expression of CCT β in metastatic tissue by IHC (Fig. 3C and D). Metastatic regions in both the lung and liver displayed more intense staining for CCT β than normal tissue. This confirmed that MDA-MB-231

Bassiouni et al.

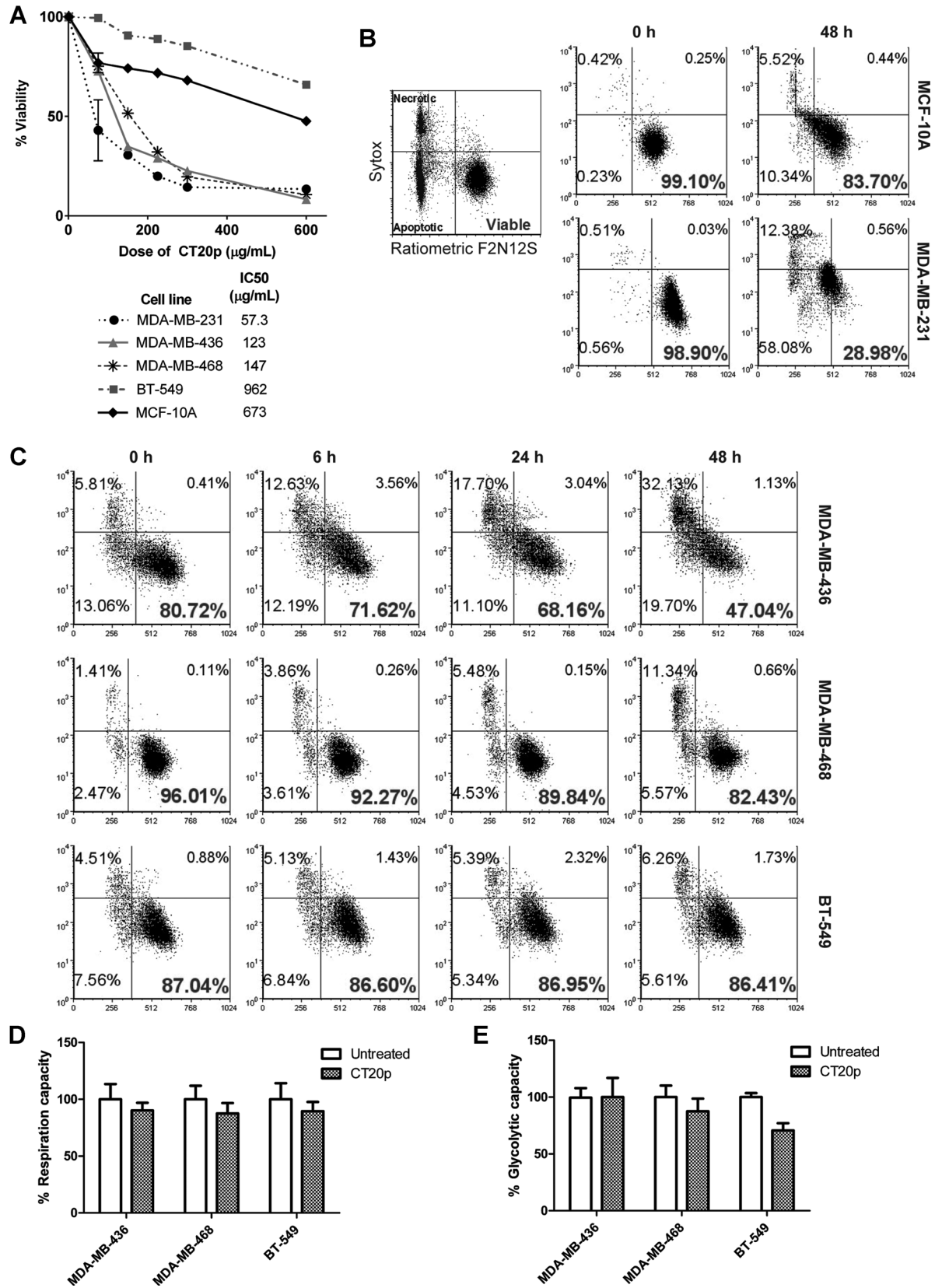
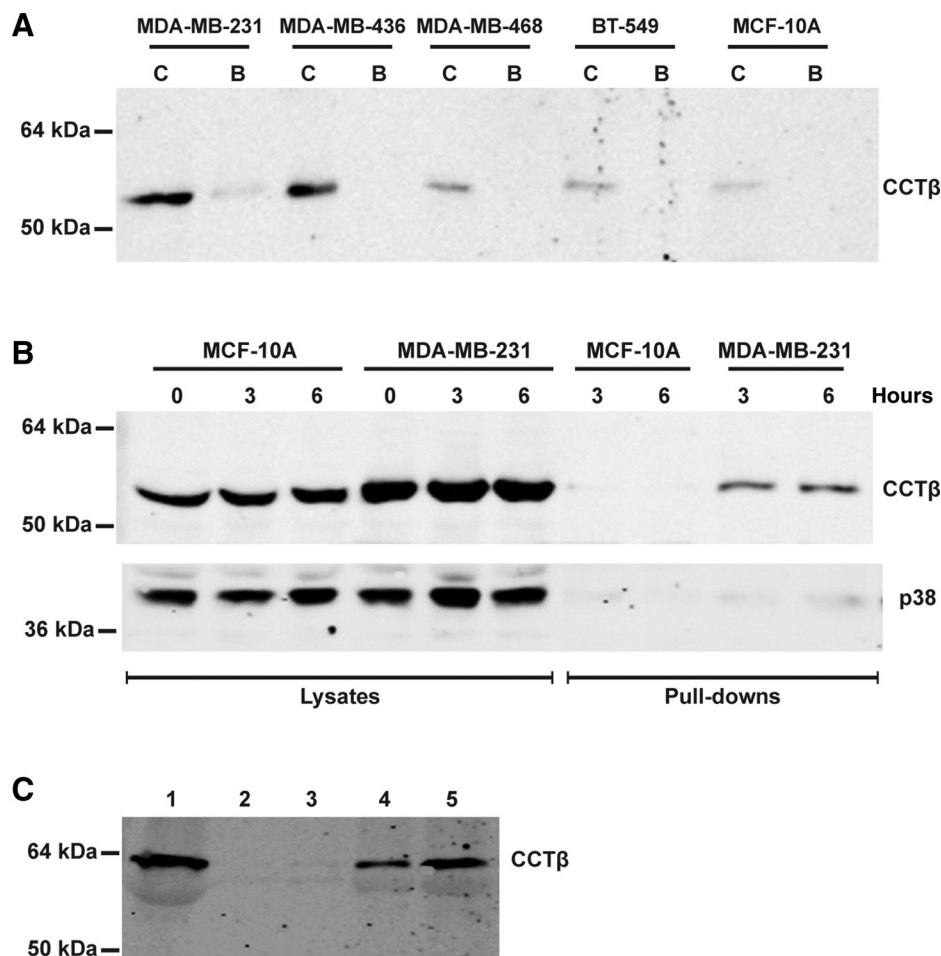


Figure 2.

CT20p binds CCT β in the cellular environment. **A**, biotin-CT20p (denoted **C**) was used to pull-down interacting proteins in TNBC cell lysates as described in Materials and Methods. Biotin only (denoted **B**) was used as a control in each cell lysate. Pull downs were analyzed by immunoblotting for CCT β . **B**, an "in-cell" pull down was performed in MDA-MB-231 and MCF-10A cells as described in Materials and Methods. Briefly, CT20p-biotin encapsulated in HBPE-NPs was delivered to viable cells, followed by cell lysis and recovery of interacting proteins. Pull downs, as well as whole-cell lysate samples, were analyzed, and CCT β and p38 were detected by Western blotting. **C**, biotin-CT20p was used to pull down His-tagged recombinant CCT β , and the results were analyzed by immunoblotting for CCT β . Lane 1 contains 0.1 nmol CCT β , the amount used for all the pull-downs. Lane 2 is a pull-down with biotin alone and serves as a negative control. Lanes 3, 4, and 5 are pull-downs with 0.1, 1, and 4 nmol Biotin-CT20p, respectively.



cells retained high-level and prolonged expression of CCT β in an *in vivo* environment.

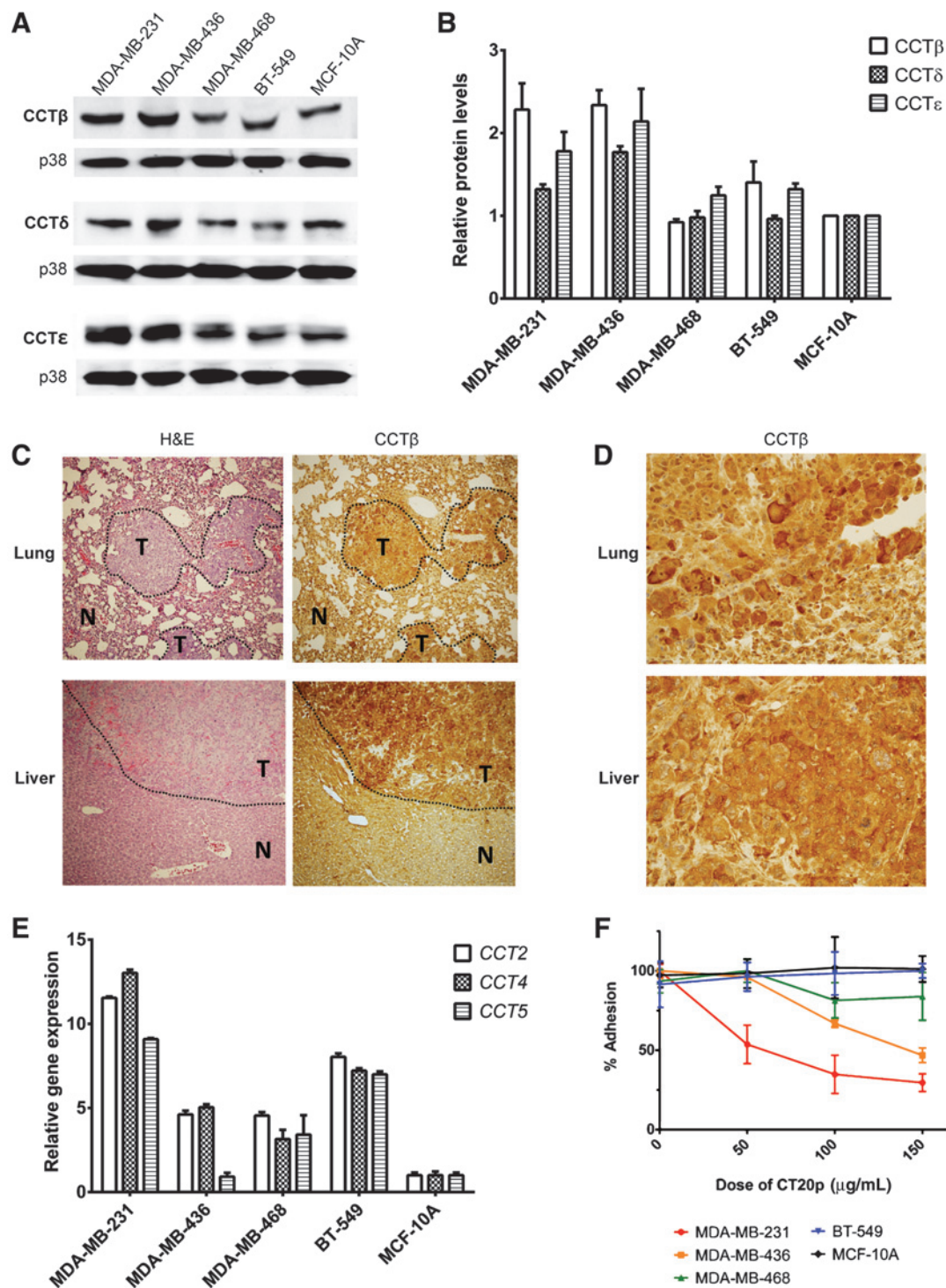
CCT gene expression was examined by RT-PCR for the three subunits assessed above in the TNBC and control cell lines (Fig. 3E). While all the TNBC cell lines expressed higher mRNA levels of the CCT subunits than the MCF-10A cells, relative gene and protein expression did not necessarily correlate, most notably in the case of BT-549 and MDA-MB-436 cells. Other groups also observed that CCT gene expression did not always correlate with protein activity (17). Hence, control of CCT gene expression by cells is likely complex and involves additional regulatory components yet to be determined.

As our data indicated that susceptibility to CT20p could correlate with the amount of cellular CCT protein and perhaps activity, rather than the transcript level, we assessed a functional consequence of CCT inhibition—cellular detachment. To assess adhesion, TNBC cells were treated with CT20p-HBPE-NPs at varying doses and adhesion measured at the endpoint of 48 hours (Fig. 3F). CT20p-HBPE-NPs caused a dose-dependent loss of adhesion, most notable in the MSL subtype cell lines, MDA-MB-231 and MDA-MB-436, correlating with both the IC₅₀ values (Fig. 1A), cell death (Fig. 1C), and the high CCT protein levels these cell lines displayed (Fig. 3A).

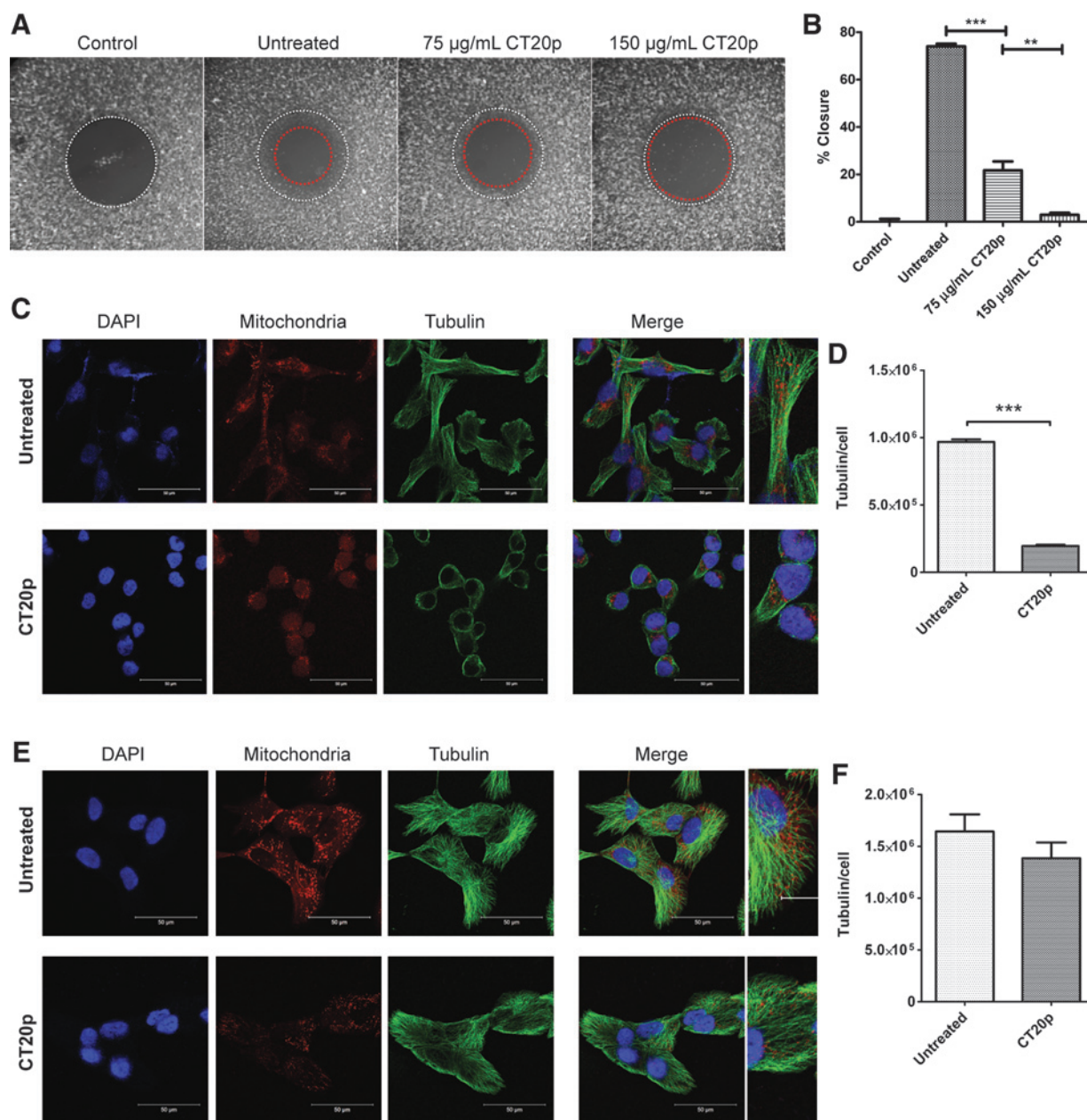
Figure 1.

CT20p has cytotoxic activity in TNBC cell lines. **A**, TNBC cell lines and a control breast epithelial line (MCF-10A) were treated with CT20p at increasing doses for 48 hours, then assessed with a luciferase-based viability assay as described in Materials and Methods. Viability was determined as a percentage relative to dose 0. IC₅₀ values were calculated as shown in Supplementary Fig. S2C and S2D. **B**, CT20p encapsulated in HBPE-NPs was delivered to MDA-MB-231 and MCF-10A cells for 48 hours as described previously (9). Cell death discrimination was achieved by staining with Sytox AADvanced and F2N12S dyes, which assesses membrane permeability and membrane asymmetry, respectively. Quadrants are displayed to divide cell populations, based on the comparison of untreated cells to a staurosporine-treated control, an example of which is shown in the key. The percentage of viable cells in the lower right quadrant is indicated in bold. As cells undergo apoptosis and necrosis, the population will lose membrane symmetry and increase permeability, shifting to the left and up. **C**, CT20p was delivered to several breast cancer cell lines for the length of time indicated in the figure, and cell viability was assessed as described in **B**. **D** and **E**, cells were treated with CT20p for 24 hours before performing metabolic stress tests (Supplementary Fig. S3), and glycolytic capacity (**D**) and mitochondrial coupling efficiency (**E**) of untreated and CT20p-treated cells were determined.

Bassiouni et al.

**Figure 3.**

CCT expression varies across TNBC cell lines. **A**, levels of three CCT subunits (beta, delta, and epsilon) were examined by Western blotting across TNBC cell lines. p38 MAP kinase is used as a loading control. **B**, protein levels of the subunits were quantified per total protein and normalized to the levels in MCF-10A cells. **C**, MDA-MB-231 metastasis in the lung and liver were obtained from NSG mice as described in Materials and Methods. Sequential tissue slices were stained with H&E and with anti-CCTβ antibody for IHC. Tumor tissue is outlined and labeled T, whereas normal tissue is labeled N. Images are taken at 100× total magnification. **D**, high magnification images of CCTβ IHC of lung and liver metastasis demonstrate the high staining intensity of tumor cells. Images are taken at 400× magnification. **E**, gene expression of the three subunits was analyzed by quantitative RT-PCR as described in Materials and Methods. The values were determined relative to MCF-10A gene expression of each subunit. The genes *CCT2*, *CCT4*, and *CCT5* correspond to CCTβ, CCTδ, and CCTε, respectively. **F**, TNBC and MCF-10A cells were treated with CT20p at increasing doses for 48 hours, and adhesion was determined using a crystal violet adhesion assay as described in Materials and Methods. The percentage of adhesion relative to dose 0 is displayed.

**Figure 4.**

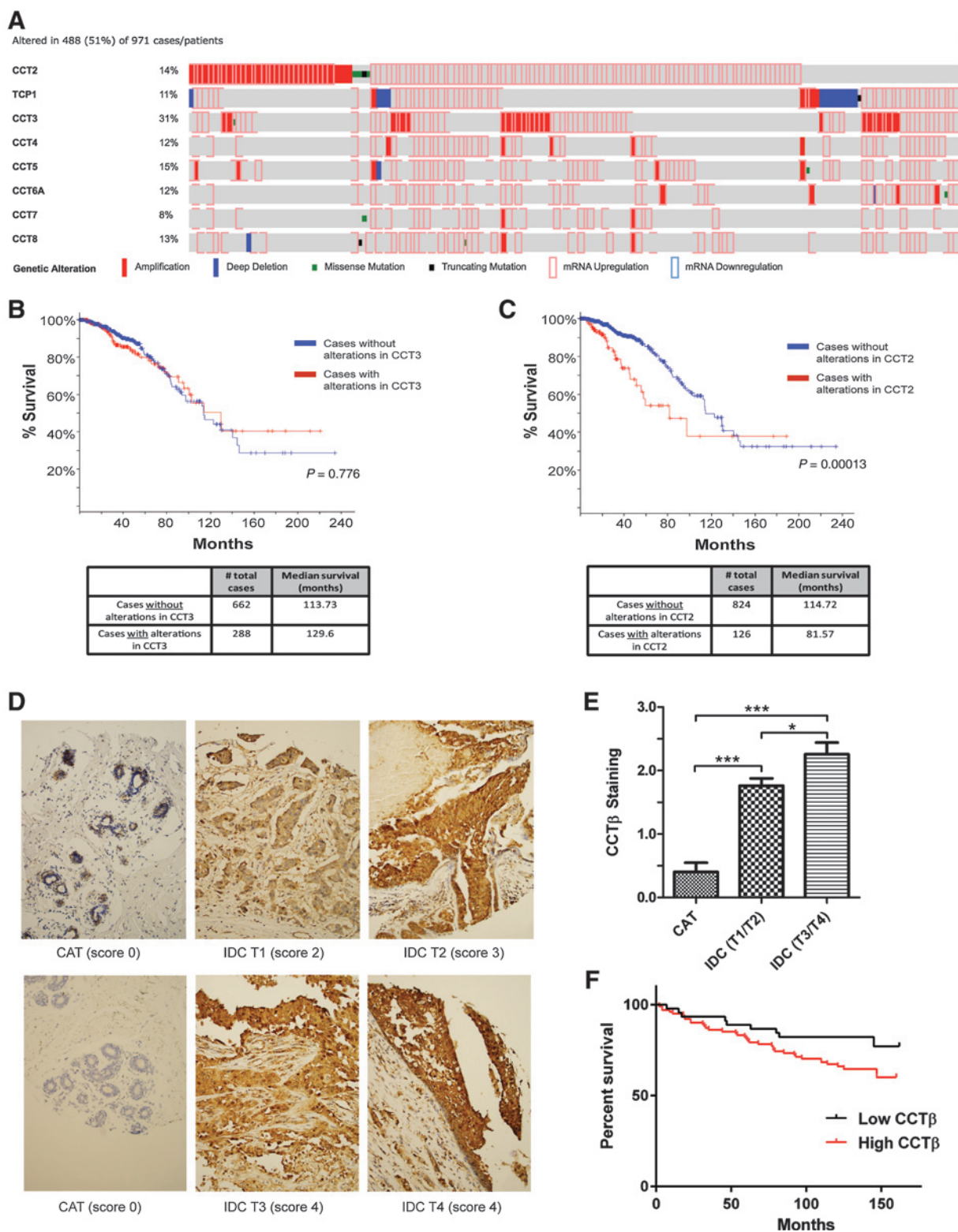
Consequences of CT20p treatment include loss of migration ability and tubulin architecture. **A**, MDA-MB-231 cells were fluorescently stained and seeded around stoppers in a 96-well plate, as described in Materials and Methods. Cells were then treated with CT20p at 75 or 150 µg/mL for 24 hours. Removal of the stoppers created an exclusion zone, outlined in white. Control cells had stoppers removed immediately before data acquisition and represent the premigration area. Remaining conditions were allowed to migrate into the exclusion zone for 10 hours before images were obtained with a Plate Runner HD. The leading edge of migrating cells after the migration period is outlined in red. **B**, migration areas were analyzed using ImageJ software, and the percentage closure of the exclusion zone was calculated as in Materials and Methods. **, $P < 0.001$; ***, $P < 0.0001$. **C–F**, MDA-MB-231 cells (**C**) and MCF-10A cells (**E**) were stained with DAPI (blue), Mitotracker Red (red), and α -DM1a antibody to tubulin (green) as described in Materials and Methods. Untreated cells were compared with cells that had been treated with CT20p for 24 hours. Tubulin architecture and mitochondrial distribution can be seen in the inset. Scale bars represent 50 µm, and inset is magnified by a factor of 2.2×. The average amount of tubulin per cell in MDA-MB-231 (**D**) and MCF-10A (**F**) cells was determined. ***, $P < 0.0001$.

CT20p's interaction with CCT has functional consequences

We previously reported that in MDA-MB-231 cells, CT20p-HBPE-NPs treatment caused loss of F-actin distribution, especially in the filopodia, and reduced integrin levels (9). As actin dynamics are necessary for cellular migration, we examined the effect of

CT20p on the motility of MDA-MB-231 cells. Cells were seeded at high density in wells containing stoppers and then treated with CT20p-HBPE-NPs for 24 hours. Stoppers were removed to create a zone of exclusion, and cells were allowed to migrate. The migration area of untreated cells was compared with those treated with

Bassiouni et al.

**Figure 5.**

CCT β is highly expressed in breast cancers and correlates with decreased survival. **A–C**, genomic analysis was performed on the Breast Invasive Carcinoma data set of TCGA (49) containing 971 cases of invasive carcinoma with sequencing and copy number analysis. **A**, genomic alterations in the eight subunits of CCT were queried, and 51% of cases were found to have alterations in at least one CCT subunit. Individually, the highest alteration rate occurred in CCT3 (31%). CCT2 was altered in 14% of cases, with the majority of these being gene amplification and mRNA upregulation. **B**, survival analysis of patients displaying CCT3 alterations revealed no association between survival rate and CCT3 alterations. (Continued on the following page.)

CT20p-HBPE-NPs at 75 and 150 $\mu\text{g}/\text{mL}$ (Fig. 4A), and percentage of closure was calculated for each condition (Fig. 4B). CT20p significantly impaired the movement of MDA-MB-231 cells in a dose-dependent manner. A comparable experiment with MCF-10A cells was limited by the fact that minimal migration of these cells is observed within a similar time frame. The migration of MCF-10A cells at a later time frame is presented in a subsequent figure.

Having previously shown that CT20p-HBPE-NP treatment caused mitochondrial clustering (9), we examined the effect of CT20p on the other main client of CCT, tubulin, which forms microtubules that move cargo like mitochondria (32). We visualized tubulin in MDA-MB-231 cells before and after 24 hours of CT20p-HBPE-NP treatment by staining cells with α -DM1A antibody specific to tubulin (pseudo-colored green). Mitotracker Red and the nuclear stain DAPI (pseudo-colored blue) were also used, and images were obtained by confocal microscopy. Apparent is the significant loss of tubulin architecture in CT20p-HBPE-NP treated cells compared with untreated cells (Fig. 4C). Decreased mitochondrial distribution is also evident but not nuclear fragmentation (Fig. 4C). Quantification of the amount of tubulin per cell confirmed a significant reduction after CT20p-HBPE-NP treatment (Fig. 4D). For comparison, we performed a parallel experiment with MCF-10A cells (Fig. 4E). Unlike MDA-MB-231 cells, there was minimal loss of tubulin per cell in MCF-10A cells (Fig. 4F), and overall cell shape and mitochondrial distribution remained normal after CT20p-HBPE-NP treatment.

The CCT β subunit displays potential as a clinical prognostic marker

We queried The Cancer Genome Atlas (TCGA) database (24, 25) for clinical breast cancer cases with genomic alterations in CCT. Alterations in the genes encoding the 8 subunits forming the CCT complex were found to occur in 51% of the breast cancer cases (Fig. 5A) with a significant probability of co-occurrence (Supplementary Fig. S6A). The genes for specific subunits displayed high alteration rates, including CCT2 (14%) and CCT3 (31%). However, when genomic alternations in these subunits were examined for impact on patient outcomes (Fig. 5B and C), CCT2 ($P = 0.00013$), but not CCT3 ($P = 0.776$), associated with a decrease in patient survival rate. Hence, alterations of the genes of individual CCT subunits may therefore have different clinical relevance. These results led to examining tissue levels of CCT2 (CCT β) using human breast cancer tissue microarrays (TMA) by IHC (Fig. 5D and Supplementary Fig. S6B). A scoring scheme for CCT β staining was developed by a pathologist and is described in Supplementary Fig. S1.

Examination of CCT β levels in cancer and normal specimens revealed that tissues from invasive ductal carcinoma (IDC) displayed staining at least three times greater than cancer-adjacent

tissue (CAT; Fig. 5E). In addition, CCT β staining was significantly increased in more highly invasive primary tumors characterized as T3 or T4 (Fig. 5E). We also examined possible connections between CCT β and the estrogen receptor (ER), progesterone receptor (PR), and HER2. With the exception of PR, we found no correlations of CCT with hormone receptors (Supplementary Fig. S6C). The PR signaling pathway could be involved in CCT expression; however, in the absence of correlations with ER, it is more likely that CCT is independent of cancer lineage markers like the hormone receptors.

Importantly, we examined survival rates of patients with IDC containing low and high levels of CCT β . Patient tissues scoring 0–2 were characterized as low expressers, and specimens scoring 3 to 4 were characterized as high expressers. Using patient data, we determined the percent survival over time between the two groups (Fig. 5F). Patients with tumors contained high CCT β exhibited a poorer outcome and survival percentage of 59.98%, whereas the low CCT β group had a more favorable survival percentage of 77.03% (Fig. 5F). These results support the findings in Fig. 5C that alternations in CCT2 gene accompany poor patient outcomes.

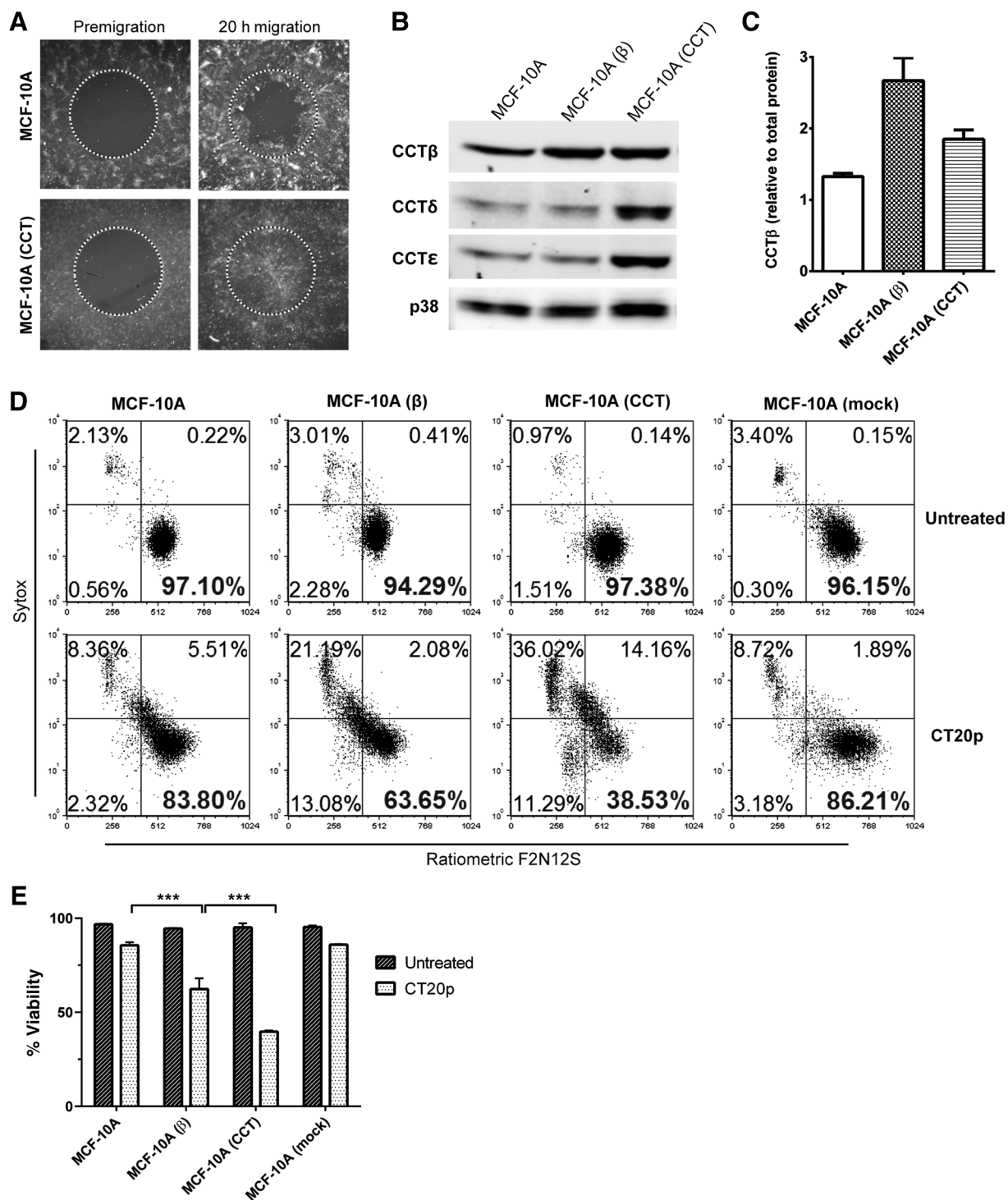
CCT β overexpression enhances susceptibility to CT20p

Having established that MCF-10A cells were more resistant to CT20p cytotoxicity (Fig. 1A), we determined whether increasing CCT β in these cells could enhance susceptibility to CT20p. MCF-10A cells can be highly sensitive to cell confluency and, when grown sparsely, will spontaneously undergo an epithelial-to-mesenchymal transition (EMT)-like process (33). We cultured MCF-10A cells at suboptimal confluency until phenotypic changes were observed. The transitioned MCF-10A cells, referred to as MCF-10A (CCT), exhibited increased migration, indicating that MCF-10A (CCT) cells had acquired migratory characteristics (Fig. 6A). We also transiently overexpressed CCT2 (CCT β) in MCF-10A cells, referred to as MCF-10A (β).

We confirmed that MCF-10A (β) and MCF-10A (CCT) cells expressed higher levels of CCT β than MCF-10A cells (Fig. 6B and C). MCF-10A (CCT) cells also contained high levels of CCT δ and CCT ϵ , indicating that these cells had likely overexpressed the entire CCT complex. Transfection of MCF-10A with the CCT2 gene did not increase the other subunits, a phenomenon previously reported in yeast (34). We examined viability of the MCF-10A variants after 24 hours of CT20p-HBPE-NP treatment (75- μg nanoparticles/mL). MCF-10A cells exhibited a minimal decrease in viability (Fig. 6D and E), whereas both MCF-10A (β) and MCF-10A (CCT) cells were more susceptible to CT20p cytotoxicity with viability decreasing to 64% and 39%, respectively (Fig. 6D and E). As a control, MCF-10A cells were mock transfected (Fig. 6D and E). Increasing CCT β levels therefore enhanced susceptibility to CT20p in cells that were normally resistant. We were also able to increase

(Continued.) **C**, survival analysis of CCT2 revealed an association between alterations in CCT2 and a decreased median survival rate, with a 30-month difference in median survival between the two groups. **D**, human breast cancer tissue arrays were analyzed by IHC for CCT β , as explained in Materials and Methods. Tissue cores were scored by a pathologist on the basis of intensity of staining (Supplementary Fig. S1). For analysis, tissues were characterized as CAT and IDC. IDC was furthermore divided by tumor severity as T1/T2 (early) and T3/T4 (locally advanced). Representative images of CAT and IDC at various T grades are provided to illustrate varied levels of CCT β . Pathologist's score is indicated in parenthesis. Images are at 200 \times total magnification. **E**, CCT β staining was compared between CAT and IDC samples, with * indicating $P < 0.05$ and *** indicating $P < 0.0001$. **F**, human breast cancer tissue array containing samples of invasive ductal carcinoma from 146 patients was analyzed by IHC for CCT β . Survival data, including survival/deceased status and duration of monitoring in months, were provided for each tissue sample. CCT β staining intensity was scored as described in Supplementary Fig. S1. Samples scoring 0, 1, and 2 were categorized as low CCT β ($n = 45$), whereas samples scoring 3 or higher were categorized as high CCT β ($n = 101$). Percent survival was compared between these two groups. $P = 0.0608$.

Bassiouni et al.

**Figure 6.**

CCT overexpression increases the susceptibility of MCF-10A cells to CT20p. **A**, MCF-10A and MCF-10A (CCT) cells were subjected to a migration assay for 20 hours as described in Fig. 4A and in Materials and Methods. The premigration area is outlined. **B**, MCF-10A cells were transfected to overexpress CCTβ as described in Materials and Methods and are denoted here as MCF-10A (β). The levels of CCT subunits were examined by immunoblotting in these cells, as well as in MCF-10A and MCF-10A (CCT) cells. p38 MAPK is used as a loading control. **C**, level of CCTβ relative to total protein was quantified in the three MCF-10A variants. **D**, MCF-10A variants were treated with CT20p at a dose of 75 μg/mL for 24 hours. Cell death discrimination was determined by staining with Sytox AADvanced and F2N12S, followed by flow cytometry as described in Fig. 1. The viable cells are in the lower-right quadrant, and their percentage is displayed in bold. As a control, mock-transfected MCF-10A were similarly analyzed. **E**, viability data of the MCF-10A variants was quantified. ***, $P < 0.001$; ****, $P < 0.0001$.

the resistance of MDA-MB-231 cells to the cytotoxic effects of the peptide by silencing the gene for CCT2 (Supplementary Fig. S7A and S7B). In total, these results indicate that CCT is the likely target of CT20p because increasing or decreasing the levels of the CCT β subunit altered susceptibility to the peptide.

Discussion

In this study, we present evidence that CT20p mediates its cytotoxic action by inhibiting the molecular chaperone, CCT. As its mode of action, CT20p could reduce the pool CCT client proteins like actin, tubulin, or STAT3 (21, 22, 27) that are necessary for the maintenance, attachment, and survival of cancer cells, leading to cell death. As a result, treatment with CT20p could reverse resistance to anoikis, a form of cell death normally caused upon cell detachment from the extracellular matrix (ECM), and impair the EMT transition. We found that CCT levels in TNBC cell lines correlated with CT20p killing, indicating that the cytotoxicity of the peptide was independent of cancer cell lineage markers and was effective in cancers, like TNBC that lack hormone receptors. While investigating the inhibitory action of CT20p on CCT is the subject of ongoing study, we determined that CT20p makes one or more direct contacts with the CCT β subunit, which contains both ATP- and substrate-binding sites (30, 35); overexpression or inhibition of which altered susceptibility to CT20p.

We, and others, noted that CCT2 (CCT β) levels corresponded with cancer severity and decreased patient survival. A recent study reported that CCT contributed to the metastasis of breast cancer to bone by folding AIB1 (36). Another determined that the genes for CCT α and CCT β were amplified in breast cancer and necessary for cancer growth and proliferation (37). In hepatocellular carcinomas, the CCT ζ subunit acted in an oncogenic manner, correlating with increased cancer severity and poor prognosis (38). CCT β and CCT ϵ were also overexpressed in both hepatocellular and colorectal cancers (39, 40). These studies concluded, as we do, that CCT subunit expression could be an indicator of cancer progression.

In addition to the clinical potential of CCT in disease characterization, we showed that targeting CCT for inhibition with CT20p is a viable cancer treatment. For example, depletion of CCT subunits by RNA interference in cancer cell lines caused cell-cycle arrest (41). An inhibitory antibody against CCT ϵ , which modulated the folding activity of CCT, caused loss of motility and cytoskeletal disorganization (41) in manner similar to that observed with CT20p. Therapeutically inhibiting CCT would be feasible if cancer cells relied on the chaperonin more than normal cells. In support, studies in mice revealed that levels of CCT correlated to the cell's needs for CCT client proteins, especially when cells are rapidly proliferating (42, 43). In mouse cell lines, CCT expression correlated with growth rate and was regulated in a cell-cycle-dependent manner (44). In the context of cancer, this effect would be multiplied, due to proliferative demands. For example, CCT was highly expressed in cancer cells compared to noncancerous cells (17). Our work also demonstrated this principle, with the highly migratory MCF-10A (CCT) cells expressing more CCT than the original MCF-10A cell line.

CCT subunits may exhibit unique individual functions. CCT ϵ , for example, regulates actin expression via the serum response

factor pathway (45), whereas CCT δ associates with the plasma membrane and alters cell shape (46). CCT α alleviates toxicity resulting from aggregates of polyglutamine-extended huntingtin (47). Furthermore, experiments in yeast determined that overexpression of individual CCT subunit yielded unique physiologic consequences (34). Similar results were also observed when each subunit was individually mutated (48). While no unique function is attributed to CCT β , our data suggest that it may have independent functions in cancer cells, as overexpression or inhibition of this subunit was able to modulate the outcome of CT20p treatment.

In summary, CT20p is an effective cytotoxic agent for breast cancer due to its ability to cause cytoskeletal disruption and loss of cell motility, followed by cell detachment and death in cells that upregulate CCT. Intravenous delivery of CT20p encapsulated in nanoparticles could regress human tumors in mice, indicating that the peptide has potential clinical application (5, 9). Targeted nanotechnologies can enable delivery of CT20p to circulating tumor cells as well as metastatic tumor sites. Having demonstrated the links between CCT and breast cancer patient survival, determining whether the chaperone is diagnostic for other cancers will have broader implications, establishing CT20p and its inhibition of CCT as a powerful new therapeutic approach for metastatic disease.

Disclosure of Potential Conflicts of Interest

No potential conflicts of interest were disclosed.

Disclaimer

Some results presented here are in part based on data generated by TCGA Research Network.

Authors' Contributions

Conception and design: R. Bassiouni, P. Vishnubhotla, J.M. Perez, A.R. Khaled

Development of methodology: R. Bassiouni, J.M. Perez, A.R. Khaled

Acquisition of data (provided animals, acquired and managed patients, provided facilities, etc.): R. Bassiouni, K.N. Nemeč, A. Iketani, A. Showalter, A.S. Khaled, R.W. Sprung Jr., C. Kaittanis, A.R. Khaled

Analysis and interpretation of data (e.g., statistical analysis, biostatistics, computational analysis): R. Bassiouni, K.N. Nemeč, A.S. Khaled, C. Kaittanis, J.M. Perez, A.R. Khaled

Writing, review, and/or revision of the manuscript: R. Bassiouni, A.S. Khaled, P. Vishnubhotla, C. Kaittanis, J.M. Perez, A.R. Khaled

Administrative, technical, or material support (i.e., reporting or organizing data, constructing databases): O. Flores, A.R. Khaled

Study supervision: J.M. Perez, A.R. Khaled

Acknowledgments

The authors thank D. Altomare and V. Pandey for providing NSG mice, and A. Copik and J. Oyer for flow cytometry and confocal microscopy assistance.

Grant Support

A.R. Khaled and J.M. Perez are supported by 1R01EB019288, NIBIB, NIH; and A.R. Khaled, Breast Cancer Research Foundation. Proteomics at Moffitt Cancer Center is supported by the National Cancer Institute under Award No. P30-CA076292 as a Cancer Center Support Grant (Principal Investigator: Thomas Sellers) and the Moffitt Foundation.

The costs of publication of this article were defrayed in part by the payment of page charges. This article must therefore be hereby marked *advertisement* in accordance with 18 U.S.C. Section 1734 solely to indicate this fact.

Received October 14, 2015; revised February 4, 2016; accepted February 21, 2016; published OnlineFirst March 24, 2016.

References

1. U.S. Cancer Statistics Working Group. United States Cancer Statistics: 1999–2011 Incidence and Mortality Web-based Report. Atlanta, GA: U.S. Department of Health and Human Services, Centers for Disease Control and Prevention and National Cancer Institute; 2014.
2. Ferlay J, Soerjomataram I, Dikshit R, Eser S, Mathers C, Rebelo M, et al. Cancer incidence and mortality worldwide: sources, methods and major patterns in GLOBOCAN2012. *Int J Cancer* 2015;136:E359–86.
3. Howlander N, Noone AM, Krapcho M, Garshell J, Miller D, Altekruse SF, et al. SEER cancer statistics review, 1975–2012. Bethesda, MD: National Cancer Institute. Available from: http://seer.cancer.gov/csr/1975_2012/. based on November 2014 SEER data submission, posted to the SEER web site, April 2015.
4. Lutz RJ. Role of the BH3 (Bcl-2 homology 3) domain in the regulation of apoptosis and Bcl-2-related proteins. *Biochem Soc Trans* 2000;28:51–6.
5. Boohaker RJ, Zhang G, Lee MW, Nemecek KN, Santra S, Perez JM, et al. Rational development of a cytotoxic peptide to trigger cell death. *Mol Pharm* 2012;9:2080–93.
6. Tatulian SA, Garg P, Nemecek KN, Chen B, Khaled AR. Molecular basis for membrane pore formation by Bax protein carboxyl terminus. *Biochemistry* 2012;51:9406–19.
7. Garg P, Nemecek KN, Khaled AR, Tatulian SA. Transmembrane pore formation by the carboxyl terminus of Bax protein. *Biochim Biophys Acta* 2013;1828:732–42.
8. Santra S, Kaittanis C, Perez JM. Aliphatic hyperbranched polyester: a new building block in the construction of multifunctional nanoparticles and nanocomposites. *Langmuir* 2010;26:5364–73.
9. Lee MW, Bassiouni R, Sparrow NA, Iketani A, Boohaker RJ, Moskowitz C, et al. The CT20 peptide causes detachment and death of metastatic breast cancer cells by promoting mitochondrial aggregation and cytoskeletal disruption. *Cell Death Dis* 2014;5:e1249.
10. Lee MW, Bassiouni R, Iketani A, Flores O, Perez JM, Khaled AR. The CT20 peptide: more than a piece of bax. *Can Cell Microenviron* 2014;1:e266.
11. Boohaker RJ, Lee MW, Vishnubhotla P, Perez JM, Khaled AR. The use of therapeutic peptides to target and to kill cancer cells. *Curr Med Chem* 2012;19:3794–804.
12. Lien S, Lowman HB. Therapeutic peptides. *Trends Biotechnol* 2003;21:556–62.
13. Liou AK, Willison KR. Elucidation of the subunit orientation in CCT (chaperonin containing TCP1) from the subunit composition of CCT micro-complexes. *EMBO J* 1997;16:4311–6.
14. Valpuesta JM, Martin-Benito J, Gomez-Puertas P, Carrascosa JL, Willison KR. Structure and function of a protein folding machine: the eukaryotic cytosolic chaperonin CCT. *FEBS Lett* 2002;529:11–6.
15. Chen X, Sullivan DS, Huffaker TC. Two yeast genes with similarity to TCP-1 are required for microtubule and actin function *in vivo*. *Proc Natl Acad Sci U S A* 1994;91:9111–5.
16. Miklos D, Caplan S, Mertens D, Hynes G, Pitluk Z, Kashi Y, et al. Primary structure and function of a second essential member of the heterooligomeric TCP1 chaperonin complex of yeast, TCP1 beta. *Proc Natl Acad Sci U S A* 1994;91:2743–7.
17. Boudiaf-Benmammam C, Cresteil T, Melki R. The cytosolic chaperonin CCT/TRiC and cancer cell proliferation. *PLoS One* 2013;8:e60895.
18. Thulasiraman V, Yang CF, Frydman J. *In vivo* newly translated polypeptides are sequestered in a protected folding environment. *EMBO J* 1999;18:85–95.
19. Kubota H. Function and regulation of cytosolic molecular chaperone CCT. *Vitam Horm* 2002;65:313–31.
20. Frydman J, Nimmesgern E, Erdjument-Bromage H, Wall JS, Tempst P, Hartl FU. Function in protein folding of TRiC, a cytosolic ring complex containing TCP-1 and structurally related subunits. *EMBO J* 1992;11:4767–78.
21. Yaffe MB, Farr GW, Miklos D, Horwich AL, Sternlicht ML, Sternlicht H. TCP1 complex is a molecular chaperone in tubulin biogenesis. *Nature* 1992;358:245–8.
22. Gao Y, Thomas JO, Chow RL, Lee GH, Cowan NJ. A cytoplasmic chaperonin that catalyzes beta-actin folding. *Cell* 1992;69:1043–50.
23. Albury TM, Pandey V, Gitto SB, Dominguez L, Spinel LP, Talarchek J, et al. Constitutively active Akt1 cooperates with KRas(G12D) to accelerate *in vivo* pancreatic tumor onset and progression. *Neoplasia* 2015;17:175–82.
24. Gao J, Aksoy BA, Dogrusoz U, Dresdner G, Gross B, Sumer SO, et al. Integrative analysis of complex cancer genomics and clinical profiles using the cBioPortal. *Sci Signal* 2013;6:pl1.
25. Cerami E, Gao J, Dogrusoz U, Gross BE, Sumer SO, Aksoy BA, et al. The cBio cancer genomics portal: an open platform for exploring multidimensional cancer genomics data. *Cancer Discov* 2012;2:401–4.
26. Lehmann BD, Bauer JA, Chen X, Sanders ME, Chakravarthy AB, Shyr Y, et al. Identification of human triple-negative breast cancer subtypes and pre-clinical models for selection of targeted therapies. *J Clin Invest* 2011;121:2750–67.
27. Kasembeli M, Lau WC, Roh SH, Eckols TK, Frydman J, Chiu W, et al. Modulation of STAT3 folding and function by TRiC/CCT chaperonin. *PLoS Biol* 2014;12:e1001844.
28. Trinidad AG, Muller PA, Cuellar J, Klejnot M, Nobis M, Valpuesta JM, et al. Interaction of p53 with the CCT complex promotes protein folding and wild-type p53 activity. *Mol Cell* 2013;50:805–17.
29. Kitamura A, Kubota H, Pack CG, Matsumoto G, Hirayama S, Takahashi Y, et al. Cytosolic chaperonin prevents polyglutamine toxicity with altering the aggregation state. *Nat Cell Biol* 2006;8:1163–70.
30. Llorca O, McCormack EA, Hynes G, Grantham J, Cordell J, Carrascosa JL, et al. Eukaryotic type II chaperonin CCT interacts with actin through specific subunits. *Nature* 1999;402:693–6.
31. Yang S, Zhang JJ, Huang XY. Mouse models for tumor metastasis. *Methods Mol Biol* 2012;928:221–8.
32. Heggeness MH, Simon M, Singer SJ. Association of mitochondria with microtubules in cultured cells. *Proc Natl Acad Sci U S A* 1978;75:3863–6.
33. Sarrío D, Rodríguez-Pinilla SM, Hardisson D, Cano A, Moreno-Bueno G, Palacios J. Epithelial-mesenchymal transition in breast cancer relates to the basal-like phenotype. *Cancer Res* 2008;68:989–97.
34. Kabir MA, Kaminska J, Segel GB, Bethlenny G, Lin P, Della Seta F, et al. Physiological effects of unassembled chaperonin Cct subunits in the yeast *Saccharomyces cerevisiae*. *Yeast* 2005;22:219–39.
35. Reissmann S, Joachimiak LA, Chen B, Meyer AS, Nguyen A, Frydman J. A gradient of ATP affinities generates an asymmetric power stroke driving the chaperonin TRiC/CCT folding cycle. *Cell Rep* 2012;2:866–77.
36. Chen L, Zhang Z, Qiu J, Zhang L, Luo X, Jang J. Chaperonin CCT-mediated AIB1 folding promotes the growth of ERalpha-positive breast cancer cells on hard substrates. *PLoS One* 2014;9:e96085.
37. Guest ST, Kratche ZR, Bollig-Fischer A, Haddad R, Ethier SP. Two members of the TRiC chaperonin complex, CCT2 and TCP1 are essential for survival of breast cancer cells and are linked to driving oncogenes. *Exp Cell Res* 2015;332:223–35.
38. Huang X, Wang X, Cheng C, Cai J, He S, Wang H, et al. Chaperonin containing TCP1, subunit 8 (CCT8) is upregulated in hepatocellular carcinoma and promotes HCC proliferation. *APMIS* 2014;122:1070–9.
39. Coghlin C, Carpenter B, Dundas SR, Lawrie LC, Telfer C, Murray GI. Characterization and over-expression of chaperonin t-complex proteins in colorectal cancer. *J Pathol* 2006;210:351–7.
40. Yokota S, Yamamoto Y, Shimizu K, Momoi H, Kamikawa T, Yamaoka Y, et al. Increased expression of cytosolic chaperonin CCT in human hepatocellular and colonic carcinoma. *Cell Stress Chaperones* 2001;6:345–50.
41. Grantham J, Brackley KI, Willison KR. Substantial CCT activity is required for cell cycle progression and cytoskeletal organization in mammalian cells. *Exp Cell Res* 2006;312:2309–24.
42. Kubota H, Willison K, Ashworth A, Nozaki M, Miyamoto H, Yamamoto H, et al. Structure and expression of the gene encoding mouse t-complex polypeptide (Tc-1). *Gene* 1992;120:207–15.
43. Silver LM, Kleene KC, Distel RJ, Hecht NB. Synthesis of mouse t complex proteins during haploid stages of spermatogenesis. *Dev Biol* 1987;119:605–8.
44. Yokota S, Yanagi H, Yura T, Kubota H. Cytosolic chaperonin is up-regulated during cell growth. Preferential expression and binding to tubulin at G(1)/S transition through early S phase. *J Biol Chem* 1999;274:37070–8.
45. Elliott KL, Svanstrom A, Spiess M, Karlsson R, Grantham J. A novel function of the monomeric CCTepsilon subunit connects the Serum Response Factor pathway to chaperone-mediated actin folding. *Mol Biol Cell* 2015;26:2801–9.

46. Spiess M, Echbarthi M, Svanstrom A, Karlsson R, Grantham J. Over-expression analysis of all eight subunits of the molecular chaperone CCT in mammalian cells reveals a novel function for CCTdelta. *J Mol Biol* 2015;427:2757–64.
47. Tam S, Geller R, Spiess C, Frydman J. The chaperonin TRiC controls polyglutamine aggregation and toxicity through subunit-specific interactions. *Nat Cell Biol* 2006;8:1155–62.
48. Amit M, Weisberg SJ, Nadler-Holly M, McCormack EA, Feldmesser E, Kaganovich D, et al. Equivalent mutations in the eight subunits of the chaperonin CCT produce dramatically different cellular and gene expression phenotypes. *J Mol Biol* 2010;401:532–43.
49. Ciriello G, Gatza ML, Beck AH, Wilkerson MD, Rhie SK, Pastore A, et al. Comprehensive molecular portraits of invasive lobular breast cancer. *Cell* 2015;163:506–19.

Clinical Cancer Research

Chaperonin Containing TCP-1 Protein Level in Breast Cancer Cells Predicts Therapeutic Application of a Cytotoxic Peptide

Rania Bassiouni, Kathleen N. Nemece, Ashley Iketani, et al.

Clin Cancer Res 2016;22:4366-4379. Published OnlineFirst March 24, 2016.

Updated version Access the most recent version of this article at:
doi:[10.1158/1078-0432.CCR-15-2502](https://doi.org/10.1158/1078-0432.CCR-15-2502)

Supplementary Material Access the most recent supplemental material at:
<http://clincancerres.aacrjournals.org/content/suppl/2016/03/24/1078-0432.CCR-15-2502.DC1>

Cited articles This article cites 47 articles, 11 of which you can access for free at:
<http://clincancerres.aacrjournals.org/content/22/17/4366.full#ref-list-1>

E-mail alerts [Sign up to receive free email-alerts](#) related to this article or journal.

Reprints and Subscriptions To order reprints of this article or to subscribe to the journal, contact the AACR Publications Department at pubs@aacr.org.

Permissions To request permission to re-use all or part of this article, use this link
<http://clincancerres.aacrjournals.org/content/22/17/4366>.
Click on "Request Permissions" which will take you to the Copyright Clearance Center's (CCC) Rightslink site.